2019

Irrigated pinto bean crop stress and yield assessment using ground based low altitude remote sensing technology

Rakesh Ranjan
Washington State University, rakesh.ranjan@wsu.edu

Abhilash K. Chandel
Washington State University, abhilash.chandel@wsu.edu

Lav R. Khot
Washington State University, Lav.khot@wsu.edu

Haitham Y. Bahlol
Washington State University, haitham.bhalol@wsu.edu

Jianfeng Zhou
Washington State University

See next page for additional authors

Available at www.sciencedirect.com

INFORMATION PROCESSING IN AGRICULTURE 6 (2019) 502–514

journal homepage: www.elsevier.com/locate/inpa

Irrigated pinto bean crop stress and yield assessment using ground based low altitude remote sensing technology

Rakesh Ranjan [a,1], *Abhilash K. Chandel* [a,1], *Lav R. Khot* [a,b,*], *Haitham Y. Bahlol* [a], *Jianfeng Zhou* [a], *Rick A. Boydston* [c], *Phillip N. Miklas* [c]

[a] *Department of Biological Systems Engineering, Washington State University, Pullman, WA, USA*
[b] *Center for Precision and Automated Agricultural Systems, IAREC, Washington State University, Prosser, WA, USA*
[c] *USDA-ARS Grain Legume Genetics and Physiology Research Unit, Prosser, WA USA*

ARTICLE INFO

Article history:
Received 8 June 2018
Received in revised form
15 January 2019
Accepted 21 January 2019
Available online 29 January 2019

Keywords:
Pinto bean
Multispectral imaging
Vegetation indices
Stress assessment
Yield potential

ABSTRACT

The pinto bean is one of widely consumed legume crop that constitutes over 42% of the U.S dry bean production. However, limited studies have been conducted in past to assess its quantitative and qualitative yield potentials. Emerging remote sensing technologies can help in such assessment. Therefore, this study evaluates the role of ground-based multispectral imagery derived vegetation indices (VIs) for irrigated the pinto bean stress and yield assessments. Studied were eight cultivars of the pinto bean grown under conventional and strip tillage treatments and irrigated at 52% and 100% of required evapotranspiration. Imagery data was acquired using a five-band multispectral imager at early, mid and late growth stages. Commonly used 25 broadband VIs were derived to capture crop stress traits and yield potential. Principal component analysis and Spearman's rank correlation tests were conducted to identify key VIs and their correlation (r_s) with abiotic stress at each growth stage. Transformed difference vegetation index, nonlinear vegetation index (NLI), modified NLI and infrared percentage vegetation index (IPVI) were consistent in accounting the stress response and crop yield at all growth stages ($r_s > 0.60$, coefficient of determination (R^2): 0.50–0.56, $P < 0.05$). Ten other VIs significantly accounted for crop stress at early and late stages. Overall, identified key VIs may be helpful to growers for precise crop management decision making and breeders for crop stress response and yield assessments.

1. Introduction

High yielding crop varieties with a significant level of tolerance towards stresses induced by disease, pests, climate change, water shortage and reduced soil fertility have been recognized as crucial needs to feed the burgeoning population

* Corresponding author at: Department of Biological Systems Engineering, Washington State University, Pullman, WA, USA.
E-mail address: lav.khot@wsu.edu (L.R. Khot).
[1] Equal contribution authors.
Peer review under responsibility of China Agricultural University.
https://doi.org/10.1016/j.inpa.2019.01.005

[1–3]. In this regard, focus has been towards increasing crop yield through timely and precision management of crop inputs [4,5]. However, majorly existing techniques to manage crop stressors have been time-consuming, labor-intensive and most importantly destructive [6,7]. In recent times alternate non-invasive advanced sensing technologies have captured huge attention in agricultural crop production management [8–11]. Technologies such as multispectral, hyperspectral, thermal imaging and light detection and ranging (LiDAR) have been used for mapping plant photosynthesis, biomass, nutrition, water use, thermal stress and crop yield potentials [12–14]. These technologies can be integrated with aerial or ground-located platforms depending on the required scale and resolution of data acquisition. Until recently, high orbiting satellite-based sensing was limited due to frequency and resolution [15–17]. The small unmanned aerial systems (UAS) based sensing can provide a needed spatiotemporal resolution [18–20]. In addition, developing ground-based rapid sensing tools can complement the process for accurate mapping of plant characteristics [21]. Such sensing devices can capture the effect of stress-inducing factors on crop canopy at specific wavelengths in emission spectra. Spectral information, commonly interpreted as vegetation indices (VIs) can be useful for crop growth and stress assessment [18,22].

Several research studies have been conducted to analyze the VIs related to specific crop traits [15,23,24]. Leaf area index (LAI) has been modeled as a crop growth indicator using normalized difference vegetation index (NDVI), ratio vegetation index (RVI) and perpendicular vegetation index (PVI) for soybean [25] and sunflower [26]. Similarly, the green–red vegetation index (GRVI) has been used to estimate barley biomass [27]. Crop growth and canopy coverage including atmospheric effects have been modeled using NDVI, renormalized difference vegetation index (RDVI), infrared percentage vegetation index (IPVI), normalized difference red-edge index (NDRE), visible atmospherically resistance index (VARI) and green normalized difference vegetation index (GNDVI) [28–30]. Crop chlorophyll and nitrogen content under various soil and environmental conditions have been also modeled using RVI, PVI, soil-adjusted vegetation index (SAVI), optimized soil-adjusted vegetation index (OSAVI), modified soil-adjusted vegetation index (MSAVI), enhanced vegetation index (EVI), difference vegetation index (DV), GNDVI, green difference vegetation index (GDV), medium resolution imaging spectrometer (MERIS) terrestrial chlorophyll index (MTCI), green chlorophyll index (CIG) and red-edge chlorophyll index (CIRE) [31–34]. Furthermore, for a variety of stress monitoring applications using VIs, NDVI, green simple ratio (GSR), modified simple ratio (MSR) and transformed chlorophyll absorption in reflectance index (TCARI) have been found significant in estimating photosynthesis and evapotranspiration in corn [31,35,36]. Similarly, the red-edge normalized difference vegetation index (RENDVI) has been critically used to monitor the stem water potential in pears [37]. The transformed difference vegetation index (TDVI), nonlinear vegetation index (NLI) and modified nonlinear vegetation index (MNLI) have been used as linear indicators of vegetation cover unlike NDVI and SAVI that get saturated with optical properties of soil [38,39]. Overall, crop stress (or disease) and yield forecasting models critically depend on chlorophyll content (TCARI/OSAVI) [40], biomass and growth durations [41]. The VIs based models can assist farmers and crop breeders in rapid stress assessment, trait evaluation and cultivar-specific yield prediction.

The crop stress and yield-related researches so far have covered most cereal crops, tuber crops, perennial crops, oil-producing crops, fiber crops, and vegetables. For above crops, efforts have been made to use satellite and aerial platforms based remote sensing techniques. However, efforts on making ground-based non-contact cum non-destructive tools for reliable and robust crop stress assessments are limited. Our study focus is thus on integrating an emerging multispectral optical sensing with a ground vehicle and exploring its suitability for rapid assessment of crop stress and yield potential in irrigated pinto bean (*Phaseolus vulgaris L.*). This is an important food crop consumed worldwide and accounts for 42% of the U.S. dry bean production [42]. Specifically, this study was focused on (1) assessment of stress response and yield potential of irrigated pinto bean at three different growth stages using ground-based non-contact multispectral imaging technique and (2) identification of appropriate vegetation indices and pertinent relationships to aid in such decision making process.

2. Material and methods

2.1. Experimental design

The experiment was conducted on a field (Fig. 1) planted with eight cultivars of the pinto bean at the Washington State University research farm (latitude 46.251241_N, longitude 119.738106_W) near Prosser, WA, USA. The field was initially divided into four plots of 80.10 × 12.20 m with a buffer land of 4.60 m between each plot. Two of the plots were fully irrigated (100% evapotranspiration [ET]) and remaining two plots received half of the required irrigation (52% ET), i.e. deficit irrigation. Each plot was further divided into four subplots of 18.30 × 12.20 m dimensions with a buffer land of 2.30 m between each. Two of these subplots were treated randomly with strip tillage and rest two were treated with conventional tillage. Each subplot was then divided into eight sections of 4.60 × 6.10 m to be planted with eight different pinto bean cultivars. The entire experiment was designed based on completely randomized block design (CRBD) with a total of 128 replicates where, each cultivar had 16 replications, with 4 under strip tillage and full irrigation, 4 under conventional tillage and full irrigation, 4 under strip tillage and half irrigation and 4 under conventional tillage and half irrigation. Herbicide was applied 28 days after plantation (DAP) while crops were irrigated after 30 days of emergence until maturity. The crop was harvested, and yield was quantified after 122 days of the growth cycle on September 19, 2016.

2.2. Data acquisition

The data acquisition was performed at early (54 DAP), mid (76 DAP) and late (98 DAP) growth stages. A five-band complementary metal-oxidesemiconductor (CMOS) type multispectral imager (RedEdge, MicaSense, Seattle, WA, USA) was

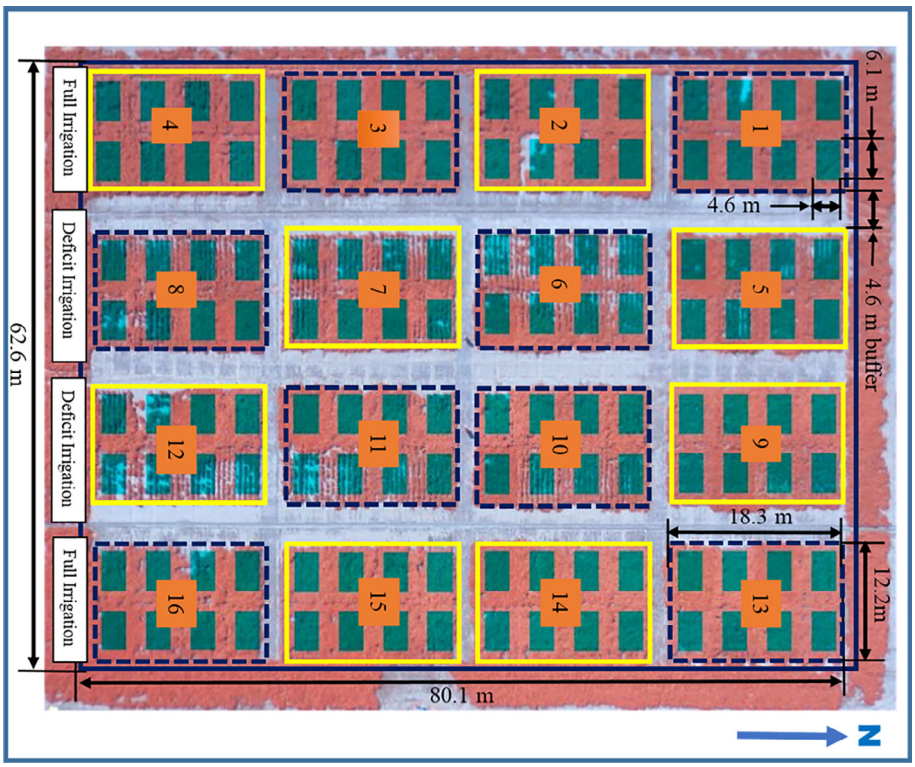

Fig. 1 – Completely randomized block design of the experimental field with 16 subplots and 8 sections planted with 8 different cultivars of the pinto bean within each subplot (total of 128). Dark blue dashed grids represent conventional tillage and solid yellow grids represent strip tillage treatments. Subplots 1, 2, 3, 4, 13, 14, 15 and 16 were treated with full irrigation while subplots 5, 6, 7, 8, 9, 10, 11 and 12 were treated with half irrigation.

employed for ground-based high resolution imaging with spectra detector bands of blue (465–485 nm), green (550–570 nm), red (663–673 nm), red-edge (RE, 712–722 nm) and near-infrared (NIR, 820–860 nm). Imager had a pixel resolution of 1280 × 960 pixels, the focal length of 5.50 mm, sensor size of 4.80 × 3.60 mm and horizontal field view of 47.20°. The imager was mounted perpendicularly on a vertically adjustable telescopic mast (LM20-S, Floatograph, Santa Barbara, CA, USA) and was set at a height of 6.70 m above ground (Fig. 2) resulting in ground sampling distance (GSD) of 4.6 mm/pixel and spatial coverage of 5.80 × 4.40 m. The mast was translocated with the help of an agricultural utility vehicle (4210, Deere & Company, Moline, IL, USA) for imaging each of 128 plot sections. The imager was powered by a universal serial bus power pack and triggered through wireless communication from a web-interface on a remote computer. Imaging was conducted around solar noon (11:00 h to 13:30 h) and data was stored in an onboard memory card. The platform was operated as stop-n-go to image each section. During the field data collection, a calibrated white reflectance panel (Active size: 15.25 × 15.25 cm, MicaSense, Seattle, WA, USA) was placed within field-of-view to adjust the spectral data for incident light variations.

Fig. 2 – (a) Ground vehicle-based setup for proximal multispectral image acquisition and (b) close-up of multispectral imager with blue, green, red, red-edge and near-infrared as five spectral bands.

2.3. *Imagery data analysis*

A total of 25 commonly used broadband VIs (Table 1) were identified as significant indicators of crop growth and yield traits under varied conditions of vegetation, environment, and soil tillage. The mean VI information was extracted through an image analysis algorithm (Fig. 3) developed in MATLAB® (ver. 2017a, The MathWorks, Inc. MA, USA). Firstly,

Table 1 – Multispectral imagery derived vegetation indices investigated in this study.

Vegetation index	Equation	Reference
Normalized Difference Vegetation Index (NDVI)	$NDVI = \frac{R_{NIR}-R_{Red}}{R_{NIR}+R_{Red}}$	[43]
Renormalized Difference Vegetation Index (RDVI)	$RDVI = \frac{R_{NIR}-R_{Red}}{\sqrt{R_{NIR}+R_{Red}}}$	[44]
Difference Vegetation Index (DV)	$DV = R_{NIR} - R_{Red}$	[45]
Soil-Adjusted Vegetation Index (SAVI)	$SAVI = (1+L) * \frac{R_{NIR}-R_{Red}}{R_{NIR}+R_{Red}+L}$	[46]
Infrared Percentage Vegetation Index (IPVI)	$IPVI = \frac{R_{NIR}}{R_{NIR}+R_{Red}}$	[28]
Green Simple Ratio (GSR)	$GSR = \frac{R_{NIR}}{R_{Green}}$	[46]
Red-Edge Normalized Difference Vegetation Index (RENDVI)	$RENDVI = \frac{R_{Red-Edge}-R_{Red}}{R_{Red-Edge}+R_{Red}}$	[47]
Non-Linear Index (NLI)	$NLI = \frac{R_{NIR}^2-R_{Red}}{R_{NIR}^2+R_{Red}}$	[38]
Modified Soil-Adjusted Vegetation Index (MSAVI)	$MSAVI = 0.5\{2R_{NIR}+1-\sqrt{X}\},\ X = (2R_{NIR}+1)^2 - 8(R_{NIR}-R_{Red})$	[48]
Modified Simple Ratio (MSR)	$MSR = (\frac{R_{NIR}}{R_{Red}}-1)/(\sqrt{\frac{R_{NIR}}{R_{Red}}}+1)$	[49]
Optimized Soil-Adjusted Vegetation Index (OSAVI)	$OSAVI = \frac{1.16*(R_{NIR}-R_{Red})}{R_{NIR}+R_{Red}+0.16}$	[50]
Green Normalized Difference Vegetation Index (GNDVI)	$GNDVI = \frac{R_{NIR}-R_{Green}}{R_{NIR}+R_{Green}}$	[51]
Transformed Difference Vegetation Index (TDVI)	$TDVI = \sqrt{0.5+\frac{R_{NIR}-R_{Red}}{R_{NIR}+R_{Red}}}$	[39]
Leaf Area Index (LAI)	$LAI = 3.618 * EVI - 0.118$	[52]
Visible Atmospherically Resistant Index (VARI)	$VARI = \frac{R_{Green}-R_{Red}}{R_{Green}+R_{Red}-R_{Blue}}$	[53]
Enhanced Vegetation Index (EVI)	$EVI = \frac{2.5*(R_{NIR}-R_{Red})}{R_{NIR}+6*R_{Red}-7.5*R_{Blue}+1}$	[54]
Red-Edge Chlorophyll Index (CIRE)	$CIRE = \frac{R_{NIR}}{R_{Red-Edge}} - 1$	[55]
Green Chlorophyll Index (CIG)	$CIG = \frac{R_{NIR}}{R_{Green}} - 1$	[56]
MERIS Terrestrial Chlorophyll Index (MTCI)	$MTCI = \frac{R_{NIR}-R_{Red-Edge}}{R_{Red-Edge}-R_{Red}}$	[57]
Green Difference Vegetation Index (GDV)	$GDV = R_{NIR} - R_{Green}$	[31]
Modified Non-Linear Index (MNLI)	$MNLI = \frac{(R_{NIR}^2-R_{Red})(1+L)}{R_{NIR}^2+R_{Red}+L}$	[58]
Green-Red Vegetation Index (GRVI)	$GRVI = \frac{R_{Green}-R_{Red}}{R_{Green}+R_{Red}}$	[59]
Ratio Vegetation Index (RVI)	$RVI = \frac{R_{NIR}}{R_{Red}}$	[60]
Normalized difference red-edge index (NDRE)	$NDRE = \frac{R_{NIR}-R_{Red-Edge}}{R_{NIR}+R_{Red-Edge}}$	[64]
Ratio Chlorophyll Absorption Reflectance (RCAR = TCARI/OSAVI)	$RCAR = \frac{3[(R_{Red-Edge}-R_{Red})-0.2(R_{Red-Edge}-R_{Green})*(R_{Red-Edge}/R_{Red})]}{[(1.16)*(R_{NIR}-R_{Red})/(R_{NIR}+R_{Red}+0.16)]}$	[40]

R_{Red}, R_{Green}, R_{Blue}, $R_{Red\text{-}Edge}$, and R_{NIR} are the pixel values of the spectral responses in red, green, blue, red-edge and NIR images.

images from all five bands were read in the algorithm and performed were a series of adjustments and alignments operations like image cropping, resizing and translation. Imagery data from all bands was then corrected by relative adjustment of pixel values with respect to the white reference panel in each image (Fig. 4). Thirdly, all the five corrected images were concatenated into RGB (R, G and B) and CIR (NIR, R, and G) images (Fig. 4). This process matches corresponding pixels in all the spectral band images to obtain a common region of interest. In the next step, the pixelated mean and mapped VIs (Fig. 5) were calculated through appropriate mathematical operations on spectral reflectance information. These were later analyzed for crop stress and yield characterization.

2.4. Data analysis

As a primary step in analysis, the data was checked for its normality. The obtained VIs were then analyzed with principal component analysis (PCA) in MATLAB® for their relationship with the yield at different growth stages. The PCA biplots were constructed with two principle axes explaining

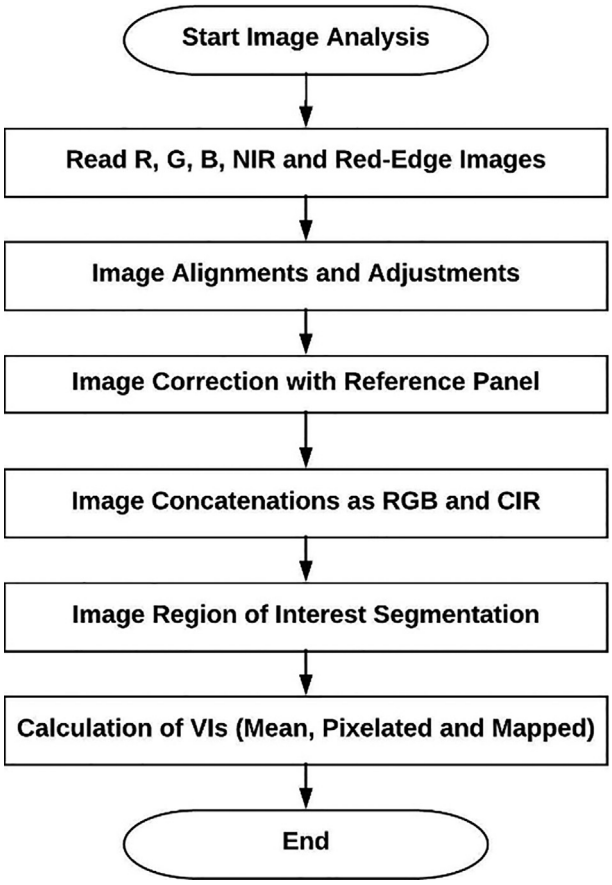

Fig. 3 – Flow chart of the multispectral image analysis algorithm.

major variability, inter-correlations and dominant pattern of VIs in the data matrix. Furthermore, linear regression models were developed, and Spearman's rank correlation test was conducted in R-Studio (Version 1.0.153, RStudio, Boston, MA, USA) to quantify yield as the function of multispectral imaging derived VIs at all the crop growth stages. The analyzed correlation coefficients were further classified into three categories as strong, moderate and weak [61]. The treatment effects of tillage and irrigation were also analyzed with two-way analysis of variance (*ANOVA*) tests and all results were inferred at 5% level of significance.

3. Results

3.1. *Salient relationships between vegetation indices and crop yield*

The PCA bi-plots assessment provided with two major principal components of VIs which at an early stage of crop growth explained a yield variability of 76% and 11%. Similarly, these axes explained a yield variability of 64% and 17% at mid-stage and 69% and 16% at the late stage. At the early stage, (Fig. 6) eigenvalues for NLI, MNLI, TDVI, IPVI, MSAVI, MSR, SAVI, NDVI, OSAVI, RVI, RDVI and DV formed a dense cluster towards extreme right and that for RENDVI lied in the right-upper region of the bi-plot. Furthermore, the eigenvalues for VARI, GRVI, and RCAR were sparsely distributed at the top-right region and CIG, GSR, NDRE, GNDVI, GDV, CIRE, and MTCI were sparsely distributed at the lower-right or right-lower region of the bi-plot. The mid-growth stage data bi-plot (Fig. 7) showed that the eigenvalues for NLI, MNLI, TDVI, IPVI, MSAVI, MSR, SAVI, NDVI, OSAVI, RVI, RDVI and DV were clustered towards extreme right and that for RENDVI lied towards the right-upper region. The VARI, GRVI, RCAR, LAI, and EVI were sparsely distributed at the top-right region and CIG, GSR, NDRE, GNDVI, GDV, CIRE and MTCI were sparsely distributed at the lower-right or right-lower region. In case of late growth stage data, bi-plot (Fig. 8) showed that the eigenvalues for NLI, MNLI, TDVI, IPVI, MSAVI, MSR, SAVI, NDVI, OSAVI, RVI, RDVI, and DVI, densely acquired the extreme right region and that for RENDVI lied towards the right-upper region. Whereas the same for VARI, GRVI, and RCAR were sparsely distributed towards the top-right region and for GDV, GNDVI, CIG, GSR, NDRE CIRE and MTCI spread in the lower-right or right-lower regions.

Overall, the VIs that are consistently clustered densely towards the extreme right region of the PCA bi-plot may be significant in accounting for the pinto bean crop stress and yield. Similarly, the indices clustered in other regions may not be considered significant in explaining the variability in response.

3.2. *Correlation of vegetation indices with potential stress and crop yield*

The results from Spearman's rank correlation analysis (Table 2) agreed strongly with the PCA results and revealed that the IPVI, TDVI, NLI, and MNLI were consistently sensitive and held a significantly positive correlation with crop yield (Spearman's correlation, $r_s = 0.60–0.62$, $p < 0.05$) at all the growth stages. Whereas, the NDVI, RDVI, DV, MSR, SAVI, MSAVI, OSAVI and RVI showed a significantly strong relationship ($r_s = 0.61–0.63$, $p < 0.05$) at the early and late stages, while a moderate ($r_s = 0.50–0.59$, $p < 0.05$) or weak ($r_s < 0.50$) relationship at mid-stage. The relationship of yield with GDV, GNDVI, and GSR varied from significantly strong at early stage ($r_s = 0.61–0.65$, $p < 0.05$) to significantly weak at mid-stage ($r_s = 0.46–0.49$, $p < 0.05$) and moderate at late stage ($r_s = 0.54–0.58$, $p < 0.05$). The VIs, EVI, LAI, CIG, VARI, GRVI, CIRE, MTCI, RENDVI and RCAR consistently depicted either moderate ($r_s = 0.50–0.59$, $p < 0.05$) or weak ($r_s < 0.50$) correlation with yield (or stress) at all three growth stages. The NDRE depicted a strong correlation only at the early stage of crop growth. Furthermore, the exponential relationships (best-fit curves) were majorly established between the stronger VIs and obtained yield (Fig. 9).

3.3. *Effect of tillage and irrigation treatments on vegetation indices and yield potential*

The analysis (Table 3) revealed that the yield of the pinto bean varied significantly with the tillage (*Two-way ANOVA*, $F_{1, 124} = 4.86$, $p = 0.049$) and irrigation treatments ($F_{1, 124} = 254.09$, $p < 0.001$). Moreover, the post-hoc analysis suggests that the yield at full irrigation (*Mean* = 5.81, standard error (*SE*) = 0.78) was significantly higher than that at half irrigation (*Tukey*

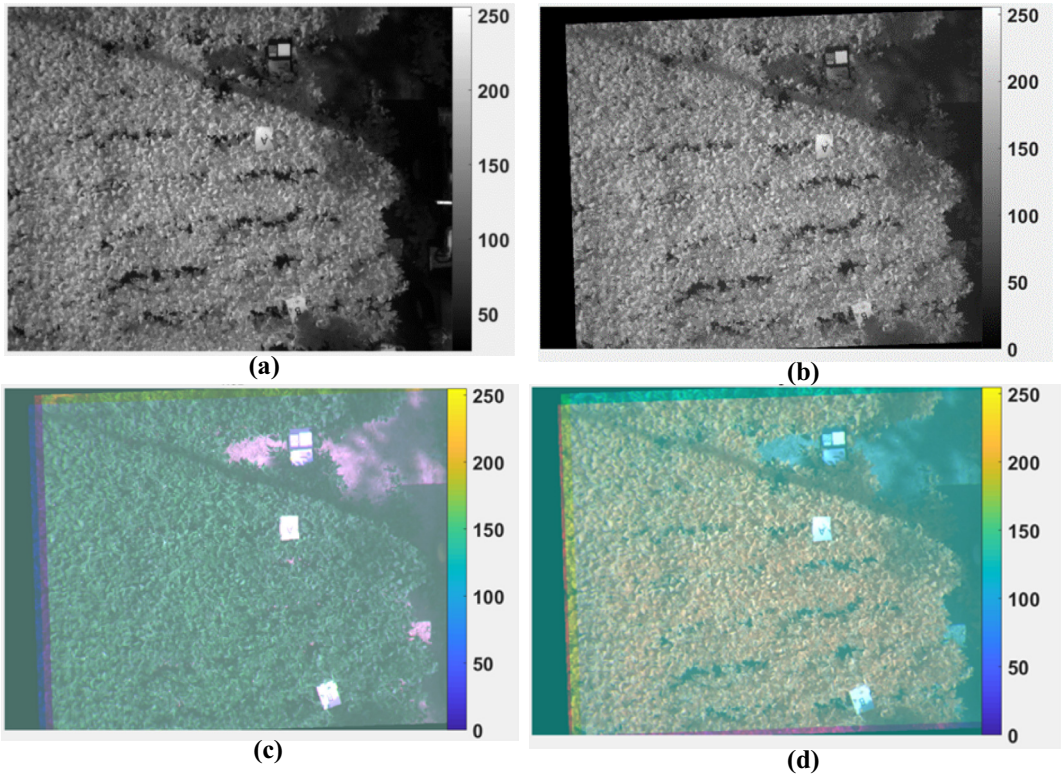

Fig. 4 – Intermediate image outputs from image analysis algorithm with (a) raw and (b) corrected near-infrared channel images and concatenated (c) RGB (Red, Green, and Blue) and (d) CIR (Red, Green, and NIR) images.

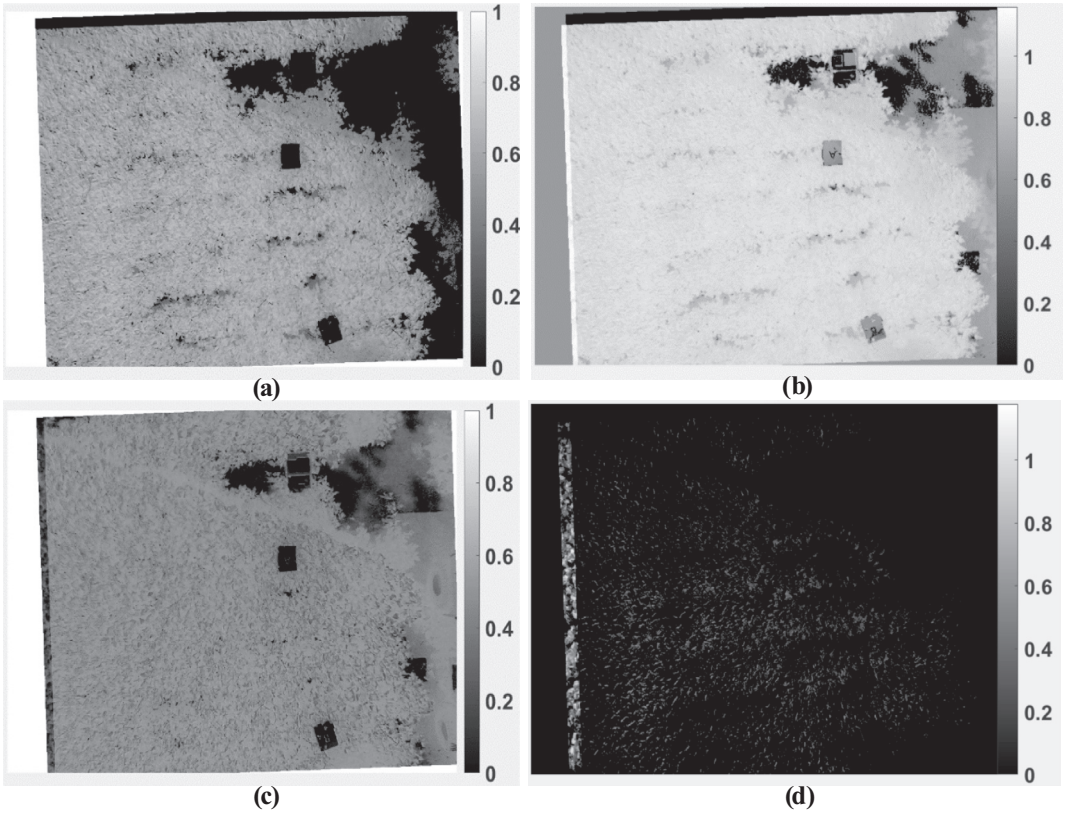

Fig. 5 – Mapped (a) NDVI, (b) TDVI, (c) GRVI and (d) CIG output images from image analysis.

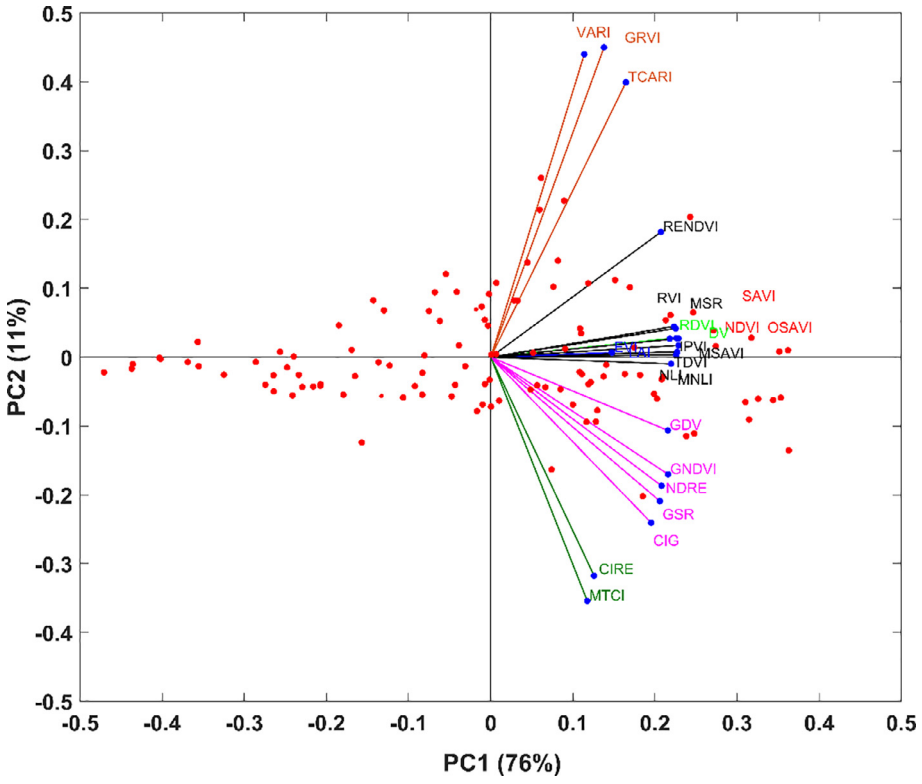

Fig. 6 – PCA bi-plot of VIs at the early stage of the Pinto bean growth period.

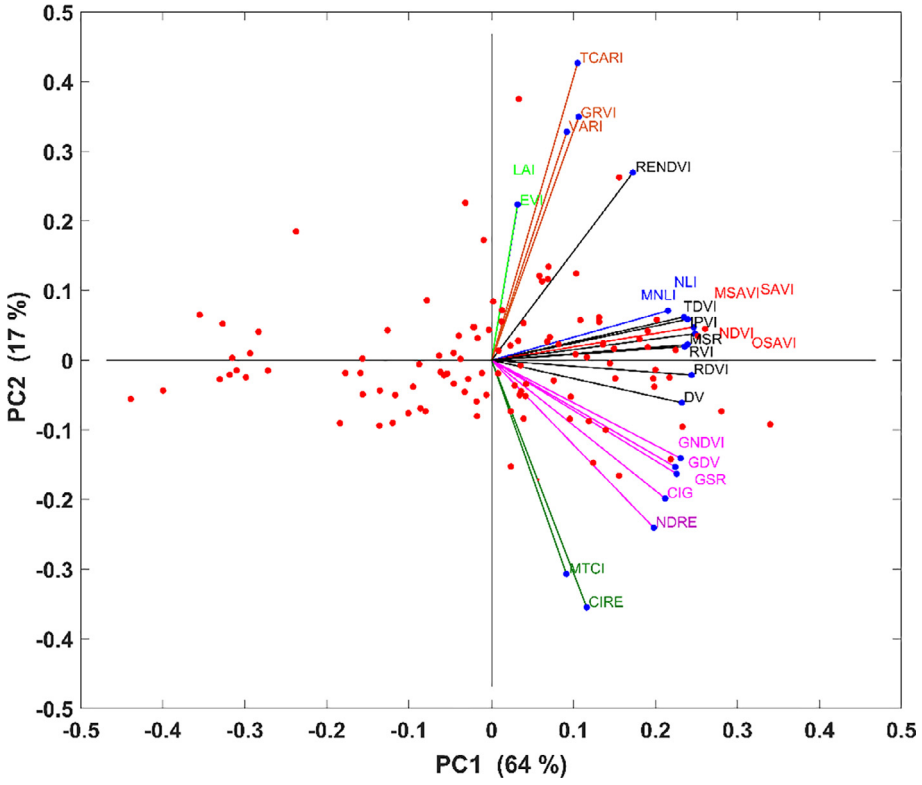

Fig. 7 – PCA bi-plot of VIs at the mid-stage of the pinto bean growth period.

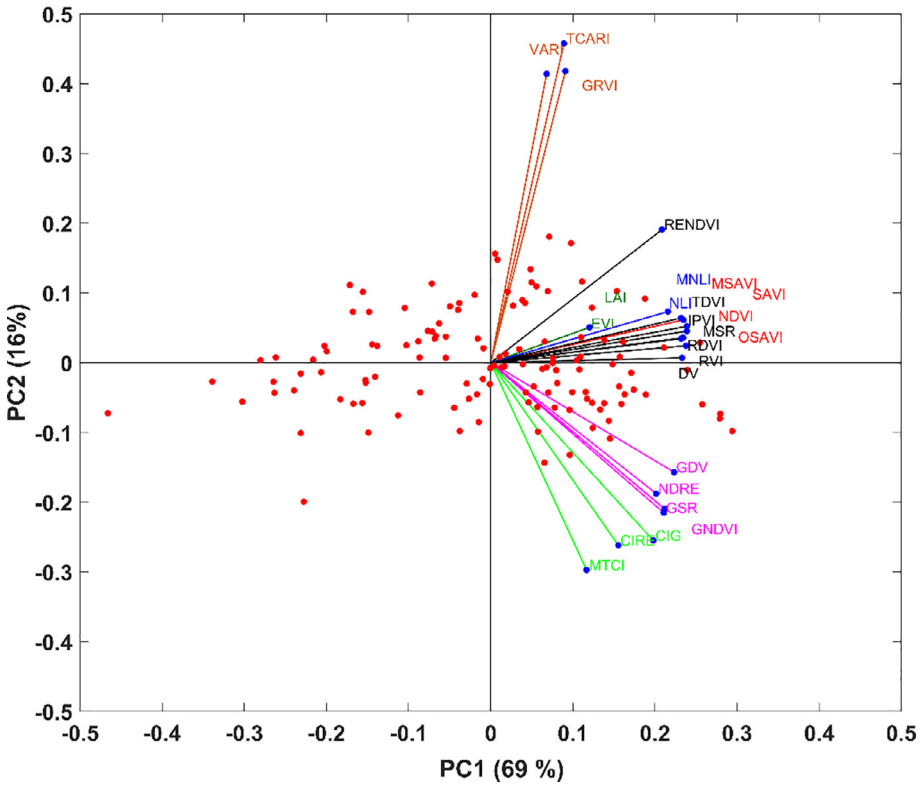

Fig. 8 – PCA bi-plot of 25 VIs at the late stage of the pinto bean growth period.

Table 2 – Correlation between different VIs and yield of the pinto bean cultivars at different growth stages.

Index	Spearman rank correlation coefficient (r_s)		
	Early stage	Mid stage	Late stage
NDVI	0.62*	0.51*	0.62*
IPVI	0.62*	0.61*	0.62*
RDVI	0.62*	0.50*	0.62*
TDVI	0.62*	0.61*	0.62*
DV	0.63*	0.48*	0.61*
GDV	0.65*	0.47*	0.58*
EVI	0.48*	0.26*	0.39*
LAI	0.48*	0.26*	0.39*
GNDVI	0.62*	0.49*	0.54*
NLI	0.61*	0.60*	0.60*
MNLI	0.61*	0.60*	0.60*
GSR	0.61*	0.46*	0.54*
MSR	0.60*	0.45*	0.61*
SAVI	0.62*	0.51*	0.62*
MSAVI	0.62*	0.52*	0.63*
OSAVI	0.62*	0.51*	0.62*
VARI	0.39*	0.13	0.21*
GRVI	0.40*	0.14*	0.26*
RENDVI	0.52*	0.44*	0.56*
NDRE	0.60*	0.30*	0.45*
CIRE	0.39*	−0.04	0.28*
CIG	0.59*	0.40*	0.49*
RVI	0.60*	0.42*	0.61*
MTCI	0.42*	0.15	0.25*
RCAR	0.43*	0.44*	0.30*

* Correlation is significant at the 0.05 level.

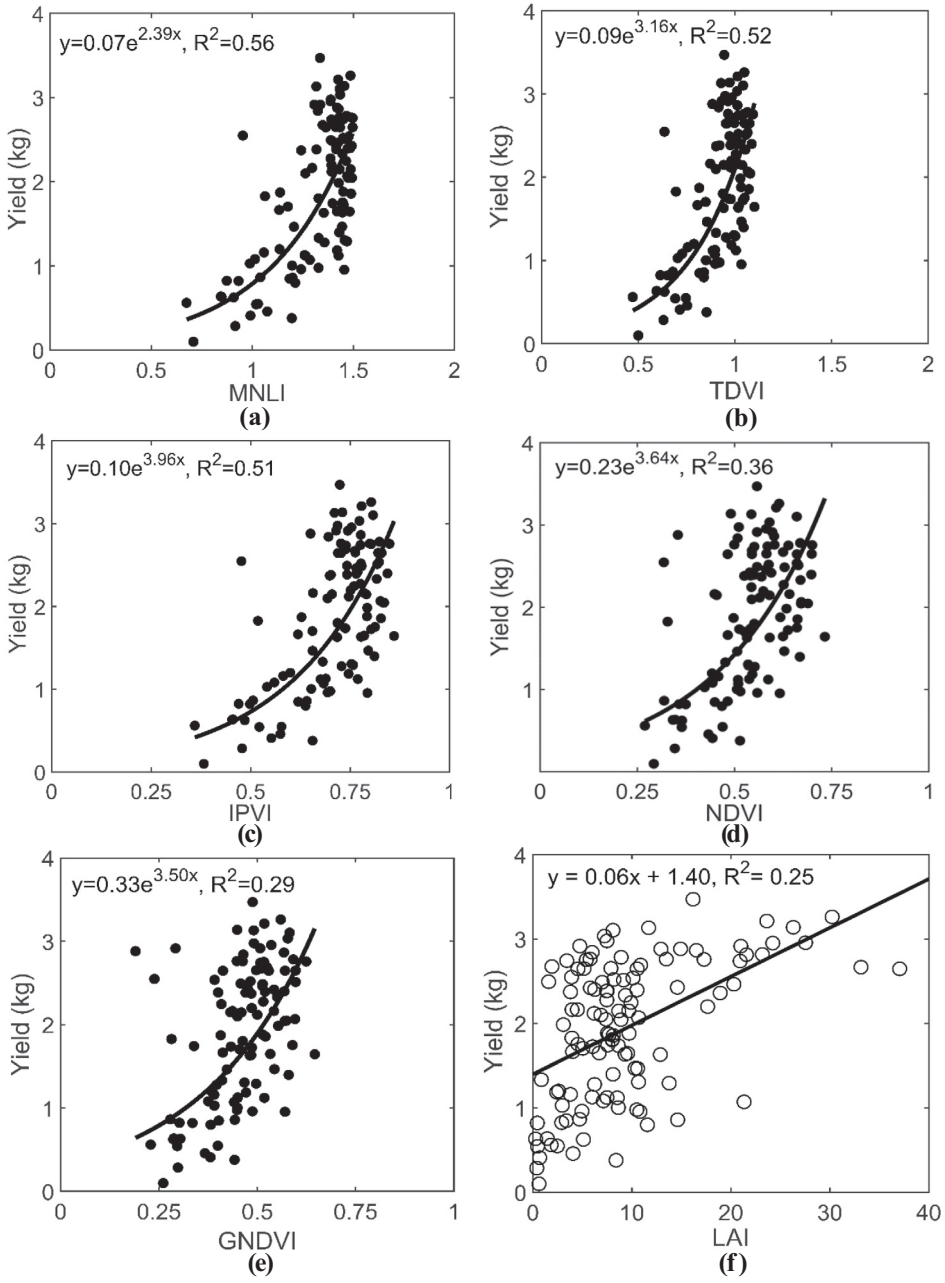

Fig. 9 – The pinto bean yield as best fit function of (a) MNLI, (b) TDVI (c) IPVI, (d) NDVI (e) GNDVI at the mid-growth stage and of (f) LAI at early stage.

HSD test, *Mean* = 2.99, *SE* = 3.17). Similarly, the yield obtained at strip tillage treatment (*Mean* = 4.59, *SE* = 1.80) was significantly higher than the yield at conventional tillage treatment (*Tukey HSD test, Mean* = 4.21, *SE* = 1.78). Note that the discussion on cultivar specific effect of tillage and irrigation treatments is beyond the scope of this work.

The analysis of VIs at all growth stages indicated that the IPVI, TDVI, NLI, MNLI, OSAVI, NDVI and GNDVI (crop vigor) were significantly affected by the irrigation treatments (*Two-way ANOVA*, $p < 0.001$) and were higher at 100% ET treatment. Additionally, the effect of tillage treatments was significant on crop vigor expressed by IPVI, TDVI, OSAVI and NDVI at early and mid-growth stages, while that on NLI and MNLI was significant at early stage only (*Two-way ANOVA*, $p < 0.05$). Furthermore, there was no prominent effect of the interaction between tillage and irrigation on crop yield and extracted VIs ($p > 0.05$).

4. Discussion

EVI and LAI in this study, deteriorated in their relationships with yield from moderate to weak with the growth stages as seen from their eigenvalues in PCA and inconsistent correlations coefficients. Thus, EVI and LAI were considered as being ineffective as compared to other VIs in accounting for crop yield and stress variations. The reason for such inconsistency

Table 3 – Effect of irrigation and tillage treatments on the pinto bean vigor expressed as vegetation indices.

Vegetation index	Growth stage	Test statistic ($F_{a,b}$)		p value		Inference	
		Irrigation	Tillage	Irrigation	Tillage	Irrigation	Tillage
IPVI	Early	0.74	0.16	<0.001	<0.001	S	S
	Mid	0.26	0.04	<0.001	0.04	S	S
	Late	0.55	0.001	<0.001	0.76	S	NS
TDVI	Early	37.20	7.70	<0.001	<0.01	S	S
	Mid	27.10	4.30	<0.001	0.04	S	S
	Late	62.66	0.07	<0.001	0.79	S	NS
NLI	Early	39.06	7.84	<0.001	<0.01	S	S
	Mid	25.20	3.60	<0.001	0.06	S	NS
	Late	48.70	0.01	<0.001	0.93	S	NS
MNLI	Early	39.06	7.84	<0.001	<0.01	S	S
	Mid	25.20	3.60	<0.001	0.06	S	NS
	Late	48.68	0.01	<0.001	0.93	S	NS
OSAVI	Early	30.50	6.73	<0.001	0.01	S	S
	Mid	23.77	4.49	<0.001	0.04	S	S
	Late	73.20	0.26	<0.001	0.61	S	NS
NDVI	Early	30.50	7.84	<0.001	<0.01	S	S
	Mid	23.77	4.49	<0.001	0.04	S	S
	Late	73.20	0.26	<0.001	0.61	S	NS
GNDVI	Early	31.05	6.94	<0.001	<0.01	S	S
	Mid	25.41	5.00	<0.001	0.03	S	S
	Late	36.12	0.12	<0.001	0.73	S	NS

'S' refers to the significant effect while 'NS' refers to the non-significant effect. The alphabet pairs (a, b) are degrees of freedom equal to (1,112) for early, (1,104) for mid and (1,123) for late stages of crop growth.

may be a low signal to noise ratio in the blue band of the spectra [62]. In this study, NLI and MNLI coincided with each other and so did the SAVI, NDVI, OSAVI, and MSAVI, depicting strong mutual correlations (or collinearity). However, MNLI can address the limitations of NLI and SAVI that are affected by optical response of the soil properties. Similarly, OSAVI [63] is capable to address the saturating nature of NDVI, SAVI and MSAVI [64]. Overall, MNLI and OSAVI may be considered solely instead of other collinear indices for efficient yield and stress assessments and eliminated cofounding effects [65]. Correlation between GNDVI and yield was found stronger at early stages, similar to couple of other studies [66,67]. However, it was weaker at later stages may be due to its stagnating nature with increased interception of photosynthetically active radiation [68]. Thus, GNDVI may be considered for crop-related management decisions only at early growth stages.

VIs such as NDVI, RDVI and OSAVI were found to either correlate strongly or moderately with the crop yield during its growth cycle. These VIs account for dynamic changes in canopy water, chlorophyll and nitrogen contents within the visible-NIR region [69–72]. In addition, a negative correlation between crop stress and yield [73] potentially depicts a strong correlation between identified VIs and stresses in the pinto bean. The spectral information from four bands viz. red (R), green (G), blue (B) and near-infrared (NIR) was sufficient for the scope of this study. The red and NIR bands provided the significant VIs viz. MNLI, NLI, TDVI etc., capable of yield and stress assessments. The difference in the significance of these VIs might be due to different combination of mathematical operators applied for their derivations. Ground-based sensing utilized in the study provides a high-resolution imagery data compared to the the satellites that may be necessary for critical crop trait assessments [74].

Overall, four VIs were strongly, and ten VIs were moderately significant in the assessment of irrigated pinto bean yield and stress. The effects of irrigation and tillage treatments on yield was successfully characterized by the identified significant VIs as supported by previous research studies [67,75].

Findings of this study may be utilized by crop breeders to determine the stress tolerant crops. Additional decisions can be made for timely and precise crop management practices for stress alleviations at an early stage and mitigate its effect or further need at mid and late stages. Overall, five band multispectral imager on-board ground platform holds a sufficient potential for robust assessments of the pinto bean yield and stress. The group of significant VIs may be analyzed by the growers and breeders to identify most suitable index for their research goals of managing a specific stress, disease or crop trait. As an advancement to this study, multispectral imager may be used on-board small UAS to assess the suitability for crop yield and stress monitoring at different altitudes and resolutions (or GSDs).

5. Conclusions

This study focused on evaluating applicability of ground based remote sensing technology for irrigated pinto bean crop response assessments during its various growth stages. Commonly used VIs derived at high spatial resolution (4.60 mm/pixel) aided in qualitative and quantitative crop assessment. Identified were the spectral band specific VIs that consistently accounted spatiotemporal crop stress response and yield

characteristics. Study followed a robust field experimentation that considered eight different cultivars, two tillage treatments, two irrigation levels and three growth stages. Results are based on reliable imagery data analysis methods with following specific conclusions.

- A five-band multispectral imager with red, green, blue, red-edge and NIR bands sufficiently acquired spectral information for consistent characterization of the pinto bean stress and crop yield potential at each of the growth stages. Most consistent VIs were obtained from the red and NIR image bands.

- Indices such as IPVI, TDVI, NLI, and MNLI clustered densely in the extreme right region of PCA bi-plots and were consistently significant in the pinto bean stress as well as yield characterization ($r_s > 0.60$ and R^2: 0.50–0.56). Additionally, NDVI, RDVI, DV, MSR, GSR, SAVI, MSAVI, OSAVI, and RVI may be used as complementary indicators. Furthermore, the consistent VIs may be inferred to significantly accommodate the effects of irrigation and tillage treatments.

Conflict of interest

The authors declare that there is no conflicts of interest.

Acknowledgments

This work was supported in part by USDA National Institute for Food and Agriculture Projects WNP00745, WNP00839 and from the Feed the Future Innovation Lab for Climate-Resilient Beans Project #AID-OAA-A-13-00077. We also thank Dr. Lynden Porter, Dr. Manoj Karkee, Mr. Encarnacion Rivera and Mr. Treva Anderson for their technical support.

REFERENCES

[1] Godfray HCJ, Beddington JR, Crute IR, Haddad L, Lawrence D, Muir JF, et al. Food security: the challenge of feeding 9 billion people. Science 2010;327:812–8.
[2] Mittler R, Blumwald E. Genetic engineering for modern agriculture: challenges and perspectives. Annu Rev Plant Biol 2010;61:443–62.
[3] Ray DK, Mueller ND, West PC, Foley JA. Yield trends are insufficient to double global crop production by 2050. PLoS One 2013;8(6):e66428.
[4] Taugourdeau S, le Maire G, Avelino J, Jones JR, Ramirez LG, Quesada MJ, et al. Leaf area index as an indicator of ecosystem services and management practices: An application for coffee agroforestry. Agric Ecosyst Environ 2014;192:19–37.
[5] Sankaran S, Khot LR, Carter AH. Field-based crop phenotyping: Multispectral aerial imaging for evaluation of winter wheat emergence and spring stand. Comput Electron Agric 2015;118:372–9.
[6] Araus JL, Cairns JE. Field high-throughput phenotyping: the new crop breeding frontier. Trends Plant Sci 2014;19:52–61.
[7] Bellvert J, Zarco-Tejada PJ, Girona J, Fereres E. Mapping crop water stress index in a 'Pinot-noir'vineyard: comparing ground measurements with thermal remote sensing imagery from an unmanned aerial vehicle. Precis Agric 2014;15(4):361–76.
[8] Chandel AK, Tewari VK, Kumar SP, Nare B, Agarwal A. On-the-go position sensing and controller predicated contact-type weed eradicator. Curr Sci 2018;114(7):1485–94.
[9] Tewari VK, Nare B, Prakash SP, Chandel AK, Tyagi A. A six-row tractor mounted microprocessor based herbicide applicator for weed control in row crops. Int Pest Control 2014;56(3):162–4.
[10] Tewari VK, Chandel AK, Nare B, Kumar SP. Sonar sensing predicated automatic spraying technology for orchards. Curr Sci 2018;115(6):1115–23.
[11] Nare B, Tewari VK, Chandel AK, Kumar SP, Chethan CR. A mechatronically integrated autonomous seed material generation system for sugarcane: A crop of industrial significance. Ind Crops Prod 2019;128:1–12.
[12] Tuberosa R. Phenotyping for drought tolerance of crops in the genomics era. Front Physiol 2012;3.
[13] van Maarschalkerweerd M, Bro R, Egebo M, Husted S. Diagnosing latent copper deficiency in intact barley leaves (Hordeum vulgare, L.) using near infrared spectroscopy. J Agric Food Chem 2013;61:10901–10.
[14] Chandel AK, Khot LR, Osroosh Y, Peters T. Thermal-RGB imager derived in-field apple surface temperature estimates for sunburn management. Agric For Meteorol 2018;254:132–40.
[15] Sankaran S, Khot LR, Espinoza CZ, Jarolmasjed S, Sathuvalli VR, Vandemark GJ, et al. Low-altitude, high-resolution aerial imaging systems for row and field crop phenotyping: A review. Eur J Agron 2015;70:112–23.
[16] Gevaert CM, Suomalainen J, Tang J, Kooistra L. Generation of spectral-temporal response surfaces by combining multispectral satellite and hyperspectral UAV imagery for precision agriculture applications. IEEE J Select Topics Appl Earth Observ Remote Sensing 2015;8:3140–6.
[17] Paek SW, Kronig LG, Ivanov AB, de Weck OL. Satellite constellation design algorithm for remote sensing of diurnal cycles phenomena. Adv Space Res 2018;62:2529–50.
[18] Zhang CH, Kovacs JM. The application of small unmanned aerial systems for precision agriculture: a review. Precis Agric 2012;13:693–712.
[19] Pena JM, Torres-Sanchez J, de Castro AI, Kelly M, Lopez-Granados F. Weed mapping in early-season maize fields using object-based analysis of unmanned aerial vehicle (UAV) images. PLoS One 2013;8:77151.
[20] Nasi R, Honkavaara E, Lyytikainen-Saarenmaa P, Blomqvist M, Litkey P, Hakala T, et al. Using UAV-Based photogrammetry and hyperspectral imaging for mapping bark beetle damage at tree-level. Remote Sens 2015;7:15467–93.
[21] Fernandez MGS, Bao Y, Tang L, Schnable PS. A high-throughput, field-based phenotyping technology for tall biomass crops. Plant Physiol 2017;174(4):2008–22.
[22] Trapp JJ, Urrea CA, Cregan PB, Miklas PN. Quantitative trait loci for yield under multiple stress and drought conditions in a dry bean population. Crop Sci 2015;55:1596–607.
[23] Zarco-Tejada PJ, Ustin S, Whiting M. Temporal and spatial relationships between within-field yield variability in cotton and high-spatial hyperspectral remote sensing imagery. Agron J 2005;97:641–53.
[24] Yang G, Liu J, Zhao C, Li Z, Huang Y, Yu H, et al. Unmanned aerial vehicle remote sensing for field-based crop phenotyping: current status and perspectives. Front Plant Sci 2017;8:1111.
[25] Lu G, Li C, Yang G, Yu H, Zhao X, Zhang X. Retrieving soybean leaf area index based on high imaging spectrometer. Soybean Sci 2016;35:599–608.

[26] Vega FA, Ramirez FC, Saiz MP, Rosua FO. Multi-temporal imaging using an unmanned aerial vehicle for monitoring a sunflower crop. Biosys Eng 2015;132:19–27.
[27] Ota T, Ogawa M, Shimizu K, Kajisa T, Mizoue N, Yoshida S, et al. Aboveground biomass estimation using structure from motion approach with aerial photographs in a seasonal tropical forest. Forests 2015;6:3882–98.
[28] Crippen RE. Calculating the vegetation index faster. Remote Sens Environ 1990;34:71–3.
[29] Gitelson AA, Kaufman YJ, Stark R, Rundquist D. Novel algorithms for remote estimation of vegetation fraction. Remote Sens Environ 2002;80:76–87.
[30] Cammarano D, Fitzgerald GJ, Casa R, Basso B. Assessing the robustness of vegetation indices to estimate, wheat N in mediterranean environments. Remote Sens 2014;6:2827–44.
[31] Sripada RP, Heiniger RW, White JG, Meijer AD. Aerial color infrared photography for determining early in-season nitrogen requirements in corn. Agron J 2006;98:968–77.
[32] Viña A, Gitelson AA, Nguy-Robertson AL, Peng Y. Comparison of different vegetation indices for the remote assessment of green leaf area index of crops. Remote Sens Environ 2011;115:3468–78.
[33] Samseemoung G, Soni P, Jayasuriya HPW, Salokhe VM. Application of low altitude remote sensing (LARS) platform for monitoring crop growth and weed infestation in a soybean plantation. Precis Agric 2012;13:611–27.
[34] Nigon TJ, Mulla DJ, Rosen CJ, Cohen Y, Alchanatis V, Knight J, Rud R. Hyperspectral aerial imagery for detecting nitrogen stress in two potato cultivars. Comp Electron Agric 2015;112:36–46.
[35] Running SW, Baldocchi DD, Turner DP, Gower ST, Bakwin PS, Hibbard KA. A global terrestrial monitoring network integrating tower fluxes, flask sampling, ecosystem modeling and EOS satellite data. Remote Sens Environ 1999;70 (1):108–27.
[36] Daughtry CST, Walthall CL, Kim MS, De Colstoun EB, McMurtrey III JE. Estimating corn leaf chlorophyll concentration from leaf and canopy reflectance. Remote Sens Environ 2000;74:229–39.
[37] Beek JV, Tits L, Somers B, Coppin P. Stem water potential monitoring in pear orchards through worldview-2 multispectral imagery. Remote Sens 2013;5:6647–66.
[38] Goel NS, Quin W. Influences of canopy architecture on relationships between various vegetation indexes and LAI and FPAR: a computer simulation. Remote Sens Environ 1994;10:309–47.
[39] Bannari A, Asalhi H, Teillet PM. Transformed difference vegetation index (TDVI) for vegetation cover mapping. In: Proc. IEEE international geoscience and remote sensing 2002 symposium. Toronto, Ontario, Canada, vol. 5; 2002. p. 3053–5.
[40] Lu S, Lu X, Zhao W, Liu Y, Wang Z, Omasa K. Comparing vegetation indices for remote chlorophyll measurement of white poplar and Chinese elm leaves with different adaxial and abaxial surfaces. J Exp Bot 2015;66(18):5625–37.
[41] Filella I, Serrano L, Serra J, Penuelas J. Evaluating wheat nitrogen status with canopy reflectance indices and discriminant analysis. Crop Sci 1995;35:1400–5.
[42] Lucier G, Lin BH, Allshouse J, Kantor LS. Factors affecting dry bean consumption in the United States. Economic Research Service, USDA, Special article 2000. p. 26–34.
[43] Rouse J, Haas R, Schell J, Deering D. Monitoring vegetation systems in the great plains with ERTS. In: Proc. third ERTS symposium, NASA, Washington D.C., USA; 1973. p. 309–17.
[44] Tucker C. Red and photographic infrared linear combinations for monitoring vegetation. Remote Sens Environ 1979;8:127–50.
[45] Huete A. A soil-adjusted vegetation index (SAVI). Remote Sens Environ 1988;25:295–309.
[46] Pinty B, Verstraete MM. GEMI: a non-linear index to monitor global vegetation from satellites. Vegetation 1992;101 (1):15–20.
[47] Gitelson A, Merzlyak M. Spectral reflectance changes associated with autumn senescence of aesculus Hippocastanum L. and acer Platanoides L. Leaves. J Plant Physiol 1994;143:286–92.
[48] Qi J, Chehbouni A, Huete AR, Kerr YH. Modified soil adjusted vegetation index (MSAVI). Remote Sens Environ 1994;48:119–26.
[49] Chen J. Evaluation of vegetation indices and modified simple ratio for boreal applications. Can J Remote Sens 1996;22:229–42.
[50] Rondeaux G, Steven M, Baret F. Optimization of soil-adjusted vegetation indices. Remote Sens Environ 1996;55:95–107.
[51] Gitelson A, Merzlyak M. Remote sensing of chlorophyll concentration in higher plant leaves. Adv Space Res 1998;22:689–92.
[52] Boegh E, Soegaard H, Broge N, Hasager C, Jensen N, Schelde K, et al. Airborne multi-spectral data for quantifying leaf area index, nitrogen concentration and photosynthetic efficiency in agriculture. Remote Sens Environ 2002;81(2–3):179–93.
[53] Gitelson A, Stark R, Grits U, Rundquist D, Kaufman YJ, Derry D. Vegetation and soil lines in visible spectral space: a concept and technique for remote estimation of vegetation fraction. Int J Remote Sens 2002;23:2537–62.
[54] Huete A, Didan K, Miura T, Rodriguez EP, Gao X, Ferreira LG. Overview of the radiometric and biophysical performance of the MODIS vegetation indices. Remote Sens Environ 2002;83:195–213.
[55] Gitelson AA, Gritz Y, Merzlyak MN. Relationships between leaf chlorophyll content and spectral reflectance and algorithms for non-destructive chlorophyll assessment in higher plant leaves. J Plant Physiol 2003;160:271–82.
[56] Gitelson AA, Viña A, Arkebauer TJ, Rundquist DC, Keydan G, Leavitt B. Remote estimation of leaf area index and green leaf biomass in maize canopies. Geophys Res Lett 2003;30:1248.
[57] Gitelson AA, Viña A, Ciganda V, Rundquist DC, Arkebauer TJ. Remote estimation of canopy chlorophyll content in crops. Geophys Res Lett 2005;32:L08403.
[58] Yang Z, Willis P, Mueller R. Impact of band-ratio enhanced AWIFS image to crop classification accuracy. In: Proceedings of the Pecora 17 remote sensing symposium denver; 2008. p. 1–11.
[59] Motohka T, Nasahara KN, Oguma H, Tsuchida S. Applicability of green-red vegetation index for remote sensing of vegetation phenology. Remote Sens 2010;2(10):2369–87.
[60] Quan Z, Xianfeng Z, Miao J. Eco-environment variable estimation from remote sensed data and eco-environment assessment: models and system. Acta Bot Sin 2011;47:1073–80.
[61] Spitkó T, Nagy Z, Zsubori ZT, Szőke C, Berzy T, Pintér J, et al. Connection between normalized difference vegetation index and yield in maize. Plant Soil Environ 2012;62(7):293–8.
[62] Jiang Z, Huete AR, Didan K, Miura R. Development of a two-band enhanced vegetation index without a blue band. Remote Sens Environ 2008;112(10):3833–45.
[63] Baret F, Jacquemoud S, Hanocq JF. About the soil line concept in remote sensing. Adv Space Res 1993;7:65–82.
[64] Leprieur C, Kerr YH, Pichon JM. Critical assessment of vegetation indices from AVHRR in a semi-arid environment. Int J Remote Sens 1996;17(13):2459–63.
[65] Pourhoseingholi MA, Baghestani AR, Vahedi M. How to control confounding effects by statistical analysis. Gastroenterol Hepatol Bed Bench 2012;5(2):79–83.
[66] Zhou J, Khot LR, Bahlol HY, Boydston R, Miklas PN. Evaluation of ground, proximal and aerial remote sensing technologies for crop stress monitoring. IFAC-PapersOnline 2016;49 (16):22–6.

[67] Zhou J, Khot LR, Boydston RA, Miklas PN, Porter L. Low altitude remote sensing technologies for crop stress monitoring: a case study on spatial and temporal monitoring of irrigated pinto bean. Precis Agric 2017;19(3):555–69.
[68] Tan C, Samanta A, Jin X, Tong L, Ma C, Guo W, et al. Using hyperspectral vegetation indices to estimate the fraction of photosynthetically active radiation absorbed by corn canopies. Int J Remote Sens 2013;34(24):8789–802.
[69] Baluja J, Diago MP, Balda P, Zorer R, Meggio F, Morales F, et al. Assessment of vineyard water status variability by thermal and multispectral imagery using an unmanned aerial vehicle (UAV). Irrig Sci 2012;30(6):511–22.
[70] Carter GA, Knapp AK. Leaf optical properties in higher plants: Linking Spectral Characteristics to Stress and Chlorophyll concentration. Am J Bot 2001;88(4):677–84.
[71] Ihuoma SO, Madramootoo CA. Recent advances in crop water stress detection. Comput Electron Agric 2017;141:267–75.
[72] Xue J, Su B. Significant remote sensing vegetation indices: a review of developments and applications. J Sensors 2017:1353691.
[73] Mickelbart MV, Hasegawa PM, Bailey-Serres J. Genetic mechanisms of abiotic stress tolerance that translate to crop yield stability. Nat Rev Genet 2015;16:237–51.
[74] Feingold G, Eberhard WL, Veron DE, Previdi M. First measurements of the twomey indirect effect using ground-based remote sensors. Geophys Res Lett 2003;30(6):1287.
[75] Boydston RA, Porter LD, Chaves-Cordoba B, Khot LR, Miklas PN. The impact of tillage on pinto bean cultivar response to drought induced by deficit irrigation. Soil Till Res 2018;180:63–72.